



Cite this: *J. Mater. Chem. C*, 2015, **3**, 10793

An organic–inorganic hybrid perovskite logic gate for better computing†

Guoming Lin,^{ab} Yuanwei Lin,^{cd} Rongli Cui,^a Huan Huang,^a Xihong Guo,^a Cheng Li,^{ab} Jinqian Dong,^a Xuefeng Guo^{ce} and Baoyun Sun^{*a}

A practicable means of significantly reducing the energy consumption and speeding up the operating rate of computer chips is to place the processor and memory into one device, which processes and stores information simultaneously like the human brain. Here we demonstrate a novel sandwich architecture where organic–inorganic hybrid perovskite materials could be used as building-block materials for non-volatile memristors, accompanied with photoresponsive performance. Owing to the distinct photo-response of the two resistance states of the memristor, it is feasible to utilize the device as a logic OR gate by employing an electrical field and light illumination as input sources. This study provides potential applications in logic circuits, optical digital computation and optical quantum information for beneficial supplementation of the von Neumann architecture, or even for computing beyond it.

Received 14th August 2015,
Accepted 9th September 2015

DOI: 10.1039/c5tc02270c

www.rsc.org/MaterialsC

The memory and processor are key components of the modern computer according to the von Neumann architecture¹ described in 1945. Due to the substantial latency of data shuttling between the memory and the processor, the closer the memory and the processor become, the better the computing which is achieved.² A two-terminal resistance switching memory component which shows a hysteretic current–voltage behavior is called a memristor (short for memory resistor),^{3–6} which has the ability to store and process information simultaneously when hybridized with complementary metal oxide semiconductor (CMOS) circuits.^{7–9} This gives hope to the possible integration of the memory and processor into one device that could go beyond the von Neumann architecture. Meanwhile, to achieve the next generation of optical digital computation or all-optical computer, with a massive parallel computing capability, low heating of junctions, high speed and high density, photons are highly recommended as the input source.¹⁰ Recently, a new class of perovskite materials with organic–inorganic hybrid components has been widely researched because it is one of the most competitive candidates

as an absorbing material for thin-film photovoltaic applications. It has certain advantages in flexibility, large-area film formation, fabrication convenience, and cheapness.¹¹ The energy conversion efficiencies reached a confirmed value of 16.2% and an unconfirmed value of 19.3% in photovoltaic cells from simple solution processes.¹² Moreover, due to the stunning exciton diffusion distances and strong photon absorbance coefficients, perovskite-material-based photodetectors^{13,14} show excellent photoconductive performances. This star-material was also reported to have memristive properties.^{15,16} Memristors that exhibit hysteresis loops in the *I–V* curve are mainly built from a simple conductor/semiconductor/conductor (CSC) thin film stack.⁷ Central semiconductor materials are traditionally metal oxides,^{17,18} chalcogenides¹⁹ and organic films.^{20–25} A perovskite material is commonly a kind of metal oxide with an ABX₃ crystal type, showing rich and colourful physical properties.^{26,27} The devices fabricated with perovskite oxides SrRuO₃,²⁸ SrTiO₃,²⁹ and CH₃NH₃PbI₃¹⁶ have been reported to have memristive properties with an ON/OFF current ratio of no more than four orders of magnitude.

Because both the photoconductive and the memristive effect have been observed in the same star-material, it offers us an opportunity of fabricating a device with a new function. Herein, a sandwich architecture, indium tin oxide (ITO)/poly(3,4-ethylenedioxythiophene)polystyrene sulfonate (PEDOT:PSS)/organic–inorganic hybrid perovskite/metal, was built. This device exhibited the functions of a memristor with the ON/OFF ratio reaching about 10⁴ at a read-out voltage of 50 mV, which is the best result of organic–inorganic hybrid perovskite based memristors. Additionally, it can achieve logic OR operation when light is switched ON/OFF and when the electrical bias is swept positive/negative. In one word, this device contains the functions of

^a CAS Key Lab for Biomedical Effects of Nanomaterials and Nanosafety, Institute of High Energy Physics, Chinese Academy of Sciences (CAS), Beijing 100049, China. E-mail: sunby@ihep.ac.cn

^b University of Chinese Academy of Sciences, Beijing 100049, China

^c Beijing National Laboratory for Molecular Sciences (BNLMS), State Key Laboratory for Structural Chemistry of Unstable and Stable Species, College of Chemistry and Molecular Engineering, Peking University, Beijing 100871, China

^d Center for Nanoscience and Nanotechnology, Academy for Advanced Interdisciplinary Studies, Peking University, Beijing 100871, China

^e Department of Advanced Materials and Nanotechnology, College of Engineering, Peking University, Beijing 100871, China

† Electronic supplementary information (ESI) available. See DOI: 10.1039/c5tc02270c

electrically controlled memory and a photo induced logic circuit (ECM & PILC) simultaneously. It has the potential of storing and processing information without data shuttling between the memory and the processor, making it a promising model for better computing that goes beyond the von Neumann architecture.

An organic–inorganic hybrid $\text{CH}_3\text{NH}_3\text{PbI}_3$ layer was fabricated by a two-step solution process and sandwiched between a PEDOT:PSS treated ITO substrate and copper (Cu) electrode as described in the experimental section. The UV-Vis absorption spectrum of the synthesized perovskite material proves that the material has a strong photon-absorbing property with a broad range from ultraviolet to near-infrared (Fig. S1a, ESI†). The X-ray diffraction (XRD) spectrum of the material indicated the formation of the perovskite structure, and no impurity peak was identified from the XRD patterns^{13,14} (Fig. S1b, ESI†). The scanning electron microscopy (SEM) image of the perovskite layer shows the continuous and full coverage of the $\text{CH}_3\text{NH}_3\text{PbI}_3$ thin film on the ITO substrate (Fig. S1c, ESI†). The atomic force microscopy (AFM) image shows that the root-mean-square (RMS) value of the $\text{CH}_3\text{NH}_3\text{PbI}_3$ thin film is 9.73 nm, revealing that the surface has a very low roughness (Fig. S1d, ESI†). All of these guarantee the respectable photoresponsive and memristive properties of the fabricated device.

A schematic diagram of the device is shown in Fig. 1a, and this architecture can be further identified by a cross-sectional SEM image (Fig. S2, ESI†). The bias was applied to the top Cu electrode, and the bottom ITO electrode was grounded. An energy diagram of the device is illustrated in Fig. 1b. The lowest unoccupied molecular orbital (LUMO) and the highest occupied molecular orbital (HOMO) levels of $\text{CH}_3\text{NH}_3\text{PbI}_3$ are -3.9 and -5.4 eV, respectively. The Fermi levels of the ITO, PEDOT:PSS and Cu electrodes are -4.7 , -4.9 and -4.65 eV, respectively. The energy level difference of PEDOT:PSS/ $\text{CH}_3\text{NH}_3\text{PbI}_3$ (HOMO) and $\text{CH}_3\text{NH}_3\text{PbI}_3$ (LUMO)/Cu were only 0.5 eV and 0.75 eV, respectively. Upon implementing a negative voltage to the Cu

electrode, the relatively small energy level difference favors the charge injections.

The I - V curve of the device with the structure of ITO/PEDOT:PSS/ $\text{CH}_3\text{NH}_3\text{PbI}_3$ /Cu shows the obvious feature of electrical bistability and the non-volatile rewritable memory effect (Fig. 1c). In detail, when the voltage was swept from zero to a negative value (with ITO as the anode and Cu as the cathode), the current density firstly showed a tendency to increase slowly and the saltation process happened at about -1 V (resistance switching from an initial high resistance state (HRS) to a low resistance state (LRS)). After that, the voltage was swept from a negative to a positive value, and the current remained high until another saltation process of current (resistance switching from LRS to HRS) happened at around $+2$ V. The device was still at a low-conductivity state during the following sweep process (from 2 V to 3 V, then to zero voltage). The resistance state was reversibly switched between LRS and HRS by sweeping the voltage repeatedly between a negative and a positive value. For the second sweep, the set voltage became -0.6 V and remained almost unchanged in the following cycles. The set process (resistance switching from HRS to LRS) occurred in the negative voltage region, whereas the reset process (resistance switching from LRS to HRS) happened at the positive voltage region, coinciding with the bipolar type of resistance switching memory.³⁰ What should be emphasized here is that the set/reset process occurs almost instantaneously in our device which is different from the results in the literature,¹⁶ suggesting that the mechanism is totally different. This process could also be expressed in the resistance–voltage curve (Fig. S3a, ESI†). It shows an obvious pinched hysteresis loop with an instantaneous set/reset process. This phenomenon could not be achieved if the device was initially swept positively (with ITO as the cathode and Cu as the anode) from 0 to 5 V. The energy barrier of PEDOT:PSS/ $\text{CH}_3\text{NH}_3\text{PbI}_3$ (LUMO) is 1 eV; the electrons could not get sufficient energy to switch the device to the ON state if ITO/PEDOT:PSS was used as the cathode.

The retention performance of the ITO/PEDOT:PSS/ $\text{CH}_3\text{NH}_3\text{PbI}_3$ /Cu device is shown in Fig. 1d. With a constant “read” voltage, the change of the conducting state of the device is an important indicator for the device stability.^{7,30} In this study, a constant “read” voltage (-50 mV) was imposed on the device at the OFF or ON state, respectively. The currents were found to be stable, with a high ON/OFF ratio of over 10^4 under the “read” voltage for a long time up to 3×10^4 s, which indicates that the device has a good stability. The endurance characterization of the device was also carried out by iteratively sweeping the voltage between 3 V and -3 V (Fig. S3b, ESI†). After aging, the device still retained the unchanged set/reset voltages and the resistance ratio stayed at a magnitude of about 10^2 . The “write–read–erase–read–rewrite” cycles could be achieved 3000 times in this study. This indicates that the storage performance of the ITO/PEDOT:PSS/ $\text{CH}_3\text{NH}_3\text{PbI}_3$ /Cu cell is good and repeatable. Similar to other non-volatile memories, the ON and OFF state of our device can be retained after removing the power supply, and rewritten many times, suggesting that the ITO/PEDOT:PSS/ $\text{CH}_3\text{NH}_3\text{PbI}_3$ /Cu sandwich device has potential applications in non-volatile random access memory (NV-RAM).

Due to the outstanding photo-responsive effect of the organic–inorganic hybrid perovskite material.^{13,14} We characterized

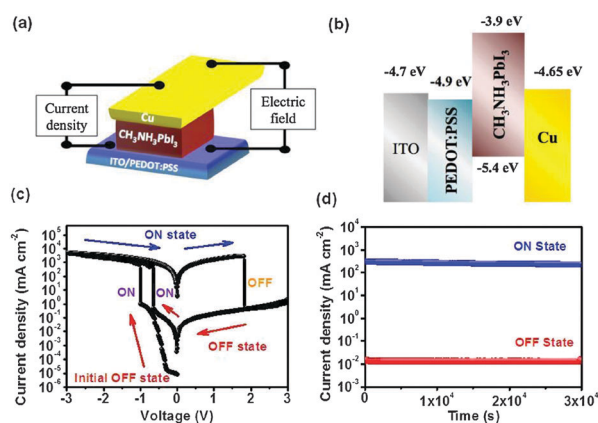


Fig. 1 Organic–inorganic hybrid perovskite memristor. (a) Schematic structure of the hybrid perovskite memristor. (b) Energy diagram of the perovskite memristor. (c) Current–voltage (I - V) characteristics of the memristor device. (d) Long-time response (*i.e.*, retention times) of the ON and OFF states of the device, probed under a constant stress of -50 mV.

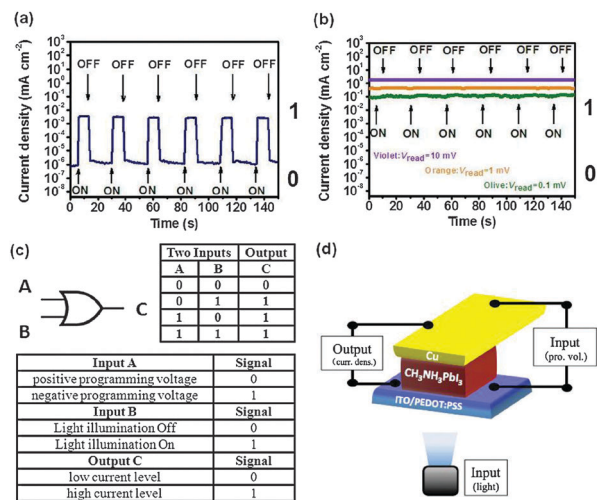


Fig. 2 Photo-induced logic OR device. (a) $I-t$ response of the device programmed to HRS under light ON/OFF switching irradiation with a read voltage of 10 mV. (b) $I-t$ response of the device programmed to LRS under light ON/OFF switching irradiation with read voltages of 0.1, 1, or 10 mV, respectively. (c) State diagram of the logic OR device with two types of input sources and one output terminal. For the input source A, which is the electrical field, signals "1" and "0" represent the negative field and the positive field, respectively. For the input source B, which is the light illumination, signals "0" and "1" represent light off and light on states, respectively. (d) Schematic diagram of the light illumination induced logic OR gate.

the photo-responsive performance of the device with the sandwich structure ITO/PEDOT:PSS/CH₃NH₃PbI₃/Cu under HRS and LRS, respectively. Fig. 2a presents six cycles of the $I-t$ response when the device stayed at HRS. The corresponding photocurrent was measured at a 10 mV bias ("read" voltage) under solar simulator irradiation (100 mW cm⁻²) switching ON/OFF for 8/18 s. It can be seen that the current density of the device stayed at HRS and could be converted from 10⁻⁶ to 10⁻³ mA cm⁻². The photo-responsive ON/OFF ratio of the device is more than 10³, and the transfer is consistent and repeatable. Fig. 2b shows the $I-t$ responses of the device at LRS, which were measured at "read" voltages of 10 mV, 1 mV and 0.1 mV, respectively. The photocurrent is hardly distinguished from the dark current at each measurement bias. In other words, the device at LRS did not show obvious photoresponse.

Consequently, a photo-induced logic OR gate was designed as showed in Fig. 2c (the inputs A and B are the electric field and light illumination, respectively, and the output C is the current level). We could define the positive electric field as the signal "0" and the negative electric field as the signal "1" for input A; the light off state as the signal "0" and light on state as the signal "1" for input B; the low current level as the signal "0" and the high current level as the signal "1" for the output C. For this device, if one or both of the inputs were signal "1", the output would always be signal "1" (high current level). On the contrary, if both of the inputs were signal "0", the output would be signal "0" (low current level). Thus, the device showed a capability of implementing logical disjunction, like a logic OR gate. The information-flow in these gates can be further achieved by an additional current-voltage converter.

To determine the origin of the electric field-induced resistance switching behaviour of the perovskite memristor, the role of the metal electrode was first explored. Cu atoms may migrate under the electric field to trigger the switching but a positive bias should be applied to the Cu electrode (with Cu as the anode) before the migration of Cu atoms.³¹ In our study, an initial set process could not be achieved if the device was initially swept positively. A negative bias is initially applied on the Cu electrode to obtain LRS, which is inconsistent with the model of migration of the Cu atoms. In addition, no metallic filament can be formed in the covalently bonded PbI₄⁻. Thus, the Cu filamentary mechanism could be excluded. The CH₃NH₃I is quite stable. The filament of carbon could not be formed in the device of ITO/PEDOT:PSS/CH₃NH₃PbI₃/Cu. To decrease the possibility of a chemical reaction at the interface of Cu/perovskite, we tested devices under the flow of N₂. The memory behavior did not show an obvious difference. Then, the conduction mechanism was investigated with the $\ln(I)-\ln(V)$ plots for HRS and LRS as depicted in Fig. 3. The slope of the LRS curve is fixed, which means that the LRS current is governed by Ohmic conduction. The slopes of the HRS curve in the high electric field and low electric field regions are 3.29 and 0.94, respectively, which suggests that the dominant conduction mechanisms of HRS were Frenkel-Poole emission in the high electric field region and Ohmic conduction in the low-electric-field region.³⁰ The linear fit of the $\ln(J/V)-V^{1/2}$ curve of HRS suggests that the electrical property was influenced by the barrier, which can be given by the expression,

$$R_c = A \exp(2aV^{1/2}/T - q\Phi_B/k_B T) \quad (1)$$

where R_c , A , k_B , q , a and T are the resistance of the interface, the prefactor, the Boltzmann constant, the electronic charge, a positive constant and temperature, respectively, which are all unchanged.

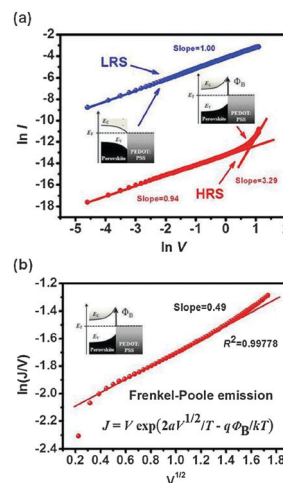


Fig. 3 Mechanism of the hybrid perovskite memristor. (a) $\ln(J)-\ln(V)$ plots of the memristor in LRS and HRS. (b) $\ln(J/V)-\ln(V)$ plots of the memristor in HRS. (Insets: Band diagrams of the CH₃NH₃PbI₃ memristor at the OFF and ON states, taking into consideration the barriers at the PEDOT:PSS/perovskite contacts. E_c , E_v and E_f are the conduction band energy, valence band energy and Fermi level energy, respectively. Φ_B is the barrier height.)

Thus, it could be inferred from expression (1) that R_c is basically dominated by the barrier height Φ_B . Therefore, the transformation of the resistance between high and low was ascribed to the variation of the barrier.

An important issue is to confirm if the barrier is situated at the PEDOT:PSS/perovskite or perovskite/Cu interface. Here we measured the I - V curves of the Cu/CH₃NH₃PbI₃/Cu, Cu/CH₃NH₃PbI₃/Au, ITO/PEDOT:PSS/CH₃NH₃PbI₃/ITO and ITO/PEDOT:PSS/CH₃NH₃PbI₃/Au structures for the control experiments (Fig. S4, ESI†). The Cu/CH₃NH₃PbI₃/Cu device kept at LRS showed no memristive phenomenon, which means that no barrier existed at the Cu/CH₃NH₃PbI₃ interface (Fig. S4a, ESI†). The Cu/CH₃NH₃PbI₃/Au device also showed no memristive phenomenon, which excluded the possibility that the memristive behaviour was generated by the asymmetric electrode (Fig. S4b, ESI†). We tested the Cu/Cu and Cu/Au devices as the control devices for the metal contact. The devices show much lower resistance than the devices of Cu/CH₃NH₃PbI₃/Cu and Cu/CH₃NH₃PbI₃/Au, which can exclude the metallic contact of the control devices of Cu/CH₃NH₃PbI₃/Cu and Cu/CH₃NH₃PbI₃/Au. To check the other interface, we measured the ITO/PEDOT:PSS/CH₃NH₃PbI₃/ITO device, and found that the memristive phenomenon still existed (Fig. S4c, ESI†). The ITO/PEDOT:PSS/CH₃NH₃PbI₃/Au device was also explored, and the unipolar memristive behaviour was similar to ref. 16. The energy level difference of CH₃NH₃PbI₃ (LUMO)/Au (Fermi level) was about 1.2 eV. Upon implementing a negative voltage to the Au electrode, the relatively high energy level difference may prevent the charge injections. Therefore, the device of ITO/PEDOT:PSS/CH₃NH₃PbI₃/Au shows no sharp set/reset voltage. As the energy level difference of CH₃NH₃PbI₃ (LUMO)/Ag (Fermi level) was only 0.3–0.4 eV, the silver may react with CH₃NH₃PbI₃ under the condition of thermal-evaporation, thus silver is not recommended. Consequently, we tend to ascribe the memristive phenomenon to the variation of the barrier on the PEDOT:PSS/CH₃NH₃PbI₃ interface, as showed in the insets of Fig. 3.

The variation of the barrier was ascribed to the change of the interface states induced by charge trapping at the metal/semiconductor interface.³² The point defects near the surface of the perovskite crystal could act as electron-trapping centers.³³ Similar to other solids, a finite concentration of point defects inevitably existed in CH₃NH₃PbI₃ at non-zero temperatures because of the configurational entropy. The density of the defect states is in the order of 1×10^{17} to $1 \times 10^{19} \text{ m}^{-3}$ in the perovskite films deposited by a solution process and thermal annealing.³³ Because of the densely packed crystal lattices of CH₃NH₃PbI₃ and other perovskite-type materials, the point defects might arise from vacancies on any of the three sublattices.

Consequently, the resistance switching behaviour could be explained by the modification of the barrier, which was induced by the charge trapping of the perovskite materials. A simplified charge-trapping model is showed in Fig. 4. At the initial state the charges were equalized at each part of the device. Due to the barrier on the PEDOT:PSS/perovskite interface, the device showed HRS (Fig. 4a). By applying a negative electric field (from ITO to the Cu electrode), charges were injected from the Cu cathode to the

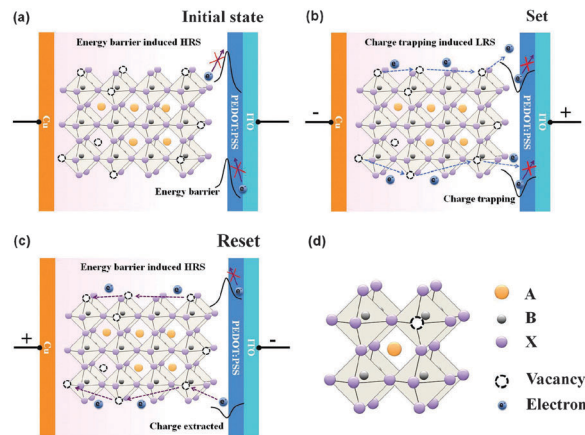


Fig. 4 Electron flowing and barrier switching under the external bias. (a) Initial HRS of the device with the barrier on the PEDOT:PSS/perovskite interface. (b) Applying a negative electric field. (c) Applying a positive electric field. (d) The perovskite crystal structure of CH₃NH₃PbI₃. A, B and X stand for CH₃NH₃, Pb and I, respectively.

perovskite material. The charge equilibrium of the initial state was broken. The barrier subsequently vanished, leading to the formation of the conducting path. Thus, the device showed LRS (Fig. 4b). Owing to the charge trapping ability of the perovskite film, even if the electric field was removed, the charges were still trapped on the perovskite material (LRS). After that, by applying a positive electric field, the charges were extracted from the perovskite film, and the barrier between the PEDOT:PSS/perovskite interface was reconstructed, which resulted in HRS of the device (Fig. 4c). When removing the electric field the barrier still existed, so the resistance stayed at a high state, and so forth.

Two other hybrid perovskite materials were further explored. We chose CH₃NH₃PbI_{3-x}Cl_x for its excellent ultra-long carrier diffusion distance³⁴ and CH₃NH₃Pb_{0.5}Sn_{0.5}I₃ for its near-infrared absorption property¹⁵ to be the representative perovskite materials. XRD spectra show that these two materials were successfully synthesized (Fig. S5, ESI†). The memristive phenomenon also exists in both the ITO/PEDOT:PSS/CH₃NH₃PbI_{3-x}Cl_x/Cu and ITO/PEDOT:PSS/CH₃NH₃Pb_{0.5}Sn_{0.5}I₃/Cu devices (Fig. S6, ESI†). This proves that by altering the constituent of the perovskite materials, the set or reset voltages, on/off ratio, *etc.* could be tuned.

To understand the mechanism of the photoresponsive phenomenon when the device stays at different resistance states (LRS and HRS), the photogain factor G is considered, which is defined by^{35,36}

$$G = \frac{\tau_c}{\tau_t} \quad (2)$$

where τ_c is the lifetime of the photogenerated carriers, and τ_t is the time required for the carriers drifting from one electrode to another. This formula can be further transformed into:³⁴

$$G = \frac{\tau_c \mu V}{l^2} \quad (3)$$

where μ , V and l are the carrier mobility of the material, the voltage applied on the device and the distance of the electrode

pair, respectively (for brevity, the derivation described in ref. 34 is not repeated here again). Note that in the photoconductive measurement, τ_c and μ are the intrinsic properties of the perovskite materials (because the memristive phenomenon is due to the change of the contact type on the perovskite/PEDOT:PSS surface, no matter if the device is at HRS or LRS, τ_c and μ of the perovskite in the bulk phase will not change), and V is kept constant to the “read” voltage. Electrode distance l is also stationary both in the programming process and the photoconductive measurement. Thus, when the device is under light illumination, the photogain is the same no matter if the device is programmed to be in an ON state or an OFF state.

On the other hand, the photogain factor G reveals how many carriers are generated per photon absorbed in the device,³⁶

$$G = \left(\frac{I_{\text{ph}}/q}{P_{\text{in}}/h\nu} \right) \times 100\% \quad (4)$$

where I_{ph} is the photo-generated current, and P_{in} is the power of the incident light beam with frequency ν . The electronic charge q and Planck's constant h are both constants. When the device is under light radiation, P_{in} stays at 100 mW cm⁻². Thus, the I_{ph} , which was determined by the difference between the photocurrent and dark-current ($I_{\text{ph}} = I_{\text{photo}} - I_{\text{dark}}$), will also be equal due to the equal photogain in both the ON state and OFF state proven in the eqn (3).

If the device is programmed to be in an OFF state before the photoconductive measurement then the dark current will stay at a low level. When photons radiate, the photo-generated current I_{ph} will produce orders of magnitude of difference between the photo-current and dark-current, as showed in Fig. 2a. Thus, the device outputs a high current level or signal “1” in the logic OR device when light illuminates, and a low current level or signal “0” when there is an absence of photon illumination. Conversely, if the device is programmed to be in an ON state before the photoconductive measurement, the dark current will stay at a high level. The same G or I_{ph} value generated by photon illumination will not produce an obvious difference between the photo-current and dark-current, making the device output at a high current level or signal “1” in the logic OR device.

Conclusions

In summary, we built a sandwich architecture, ITO/PEDOT:PSS/organic-inorganic hybrid perovskite/Cu, which contains the functions of ECM and PILC simultaneously. It exhibited excellent electrically bistable and non-volatile rewritable memory effects with an outstanding ON/OFF ratio (10^4) at a read-out voltage of 50 mV, a long retention time up to 3×10^4 s and 3000 endurance cycles, at least. The charge trapping on the point defects of the materials varied the barrier on the PEDOT:PSS/CH₃NH₃PbI₃ interface. Additionally, it showed a different photoresponse when the device stayed at different resistance states (LRS and HRS). The photo-responsive ON/OFF ratio of the device at HRS is more than 10^3 , and the transfer is consistent and repeatable, but the

photocurrent is hardly distinguished from the dark current at LRS. These phenomena have been attributed to the special structure of the new organic-inorganic hybrid perovskite. The combination of electrical programming and photo-regulation achieved logic OR operation successfully for better computing.

Acknowledgements

This work was financially supported by National Basic Research Program of China (973 Program) (2012CB932601) and National Natural Science Foundation of China (21271174, Y5118Y005C).

Notes and references

- 1 J. von Neumann, *IEEE Ann. Hist. Comput.*, 1993, **15**, 27.
- 2 H.-S. P. Wong and S. Salahuddin, *Nat. Nanotechnol.*, 2015, **10**, 191.
- 3 L. O. Chua, *Appl. Phys. A: Mater. Sci. Process.*, 2011, **102**, 765.
- 4 L. O. Chua, *IEEE Trans. Circuit Theory*, 1971, **18**, 507.
- 5 L. O. Chua and S. M. Kang, *Proc. IEEE*, 1976, **64**, 209.
- 6 D. B. Strukov, G. S. Snider, D. R. Stewart and R. S. Williams, *Nature*, 2008, **453**, 80.
- 7 J. J. Yang, D. B. Strukov and D. R. Stewart, *Nat. Nanotechnol.*, 2013, **8**, 13.
- 8 Q. Xia, W. Robinett, M. W. Cumbie, N. Banerjee, T. J. Cardinali, J. J. Yang, W. Wu, X. Li, W. M. Tong, D. B. Strukov, G. S. Snider, G. Medeiros-Ribeiro and R. S. Williams, *Nano Lett.*, 2009, **9**, 3640.
- 9 J. Borghetti, Z. Li, J. Straznicki, X. Li, D. A. A. Ohlberg, W. Wu, D. R. Stewart and R. S. Williams, *Proc. Natl. Acad. Sci. U. S. A.*, 2009, **106**, 1699.
- 10 K. Jain and G. W. Pratt, *Appl. Phys. Lett.*, 1976, **28**, 719.
- 11 Z. Xiao, Q. Dong, C. Bi, Y. Shao, Y. Yuan and J. Huang, *Adv. Mater.*, 2014, **26**, 6503.
- 12 M. A. Green, A. Ho-Baillie and H. J. Snaith, *Nat. Photonics*, 2014, **8**, 506.
- 13 L. Dou, Y. Yang, J. You, Z. Hong, W. H. Chang, G. Li and Y. Yang, *Nat. Commun.*, 2014, **5**, 5404.
- 14 X. Hu, X. Zhang, L. Liang, J. Bao, S. Li, W. Yang and Y. Xie, *Adv. Funct. Mater.*, 2014, **24**, 7373.
- 15 C. C. Stoumpos, C. D. Malliakas and M. G. Kanatzidis, *Inorg. Chem.*, 2013, **52**, 9019.
- 16 Z. Xiao, Y. Yuan, Y. Shao, Q. Wang, Q. Dong, C. Bi, P. Sharma, A. Gruverman and J. Huang, *Nat. Mater.*, 2015, **14**, 193.
- 17 C. H. Cheng, F. S. Yeh and A. Chin, *Adv. Mater.*, 2011, **23**, 902.
- 18 M. D. Pickett, J. Borghetti, J. J. Yang, G. Medeiros-Ribeiro and R. S. Williams, *Adv. Mater.*, 2011, **23**, 1730.
- 19 K. Terabe, T. Hasegawa, T. Nakayama and M. Aono, *Nature*, 2005, **433**, 47.
- 20 D. Yue, R. Cui, X. ruan, H. Huang, X. Guo, Z. Wang, X. Gao, S. Yang, J. Dong, F. Yi and B. Sun, *Org. Electron.*, 2014, **15**, 3482.
- 21 J. Li and Q. Zhang, *ACS Appl. Mater. Interfaces*, 2015, DOI: 10.1021/acsami.5b00113.

- 22 B. Hu, C. Wang, J. Wang, J. Gao, K. Wang, J. Wu, G. Zhang, W. Cheng, B. Venkateswarlu, M. Wang, P. S. Lee and Q. Zhang, *Chem. Sci.*, 2014, **5**, 3404.
- 23 C. Wang, J. Wang, P. Li, J. Gao, S. Tan, W. Xiong, B. Hu, P. S. Lee, Y. Zhao and Q. Zhang, *Chem. – Asian J.*, 2014, **9**, 779.
- 24 G. Li, K. Zheng, C. Wang, K. S. Leck, F. Hu, X. W. Sun and Q. Zhang, *ACS Appl. Mater. Interfaces*, 2013, **5**, 6458.
- 25 P. Gu, F. Zhou, J. Gao, G. Li, C. Wang, Q. Xu, Q. Zhang and J. Lu, *J. Am. Chem. Soc.*, 2013, **135**, 14086.
- 26 T. Kimura, T. Goto, H. Shintani, K. Ishizaka, T. Arima and Y. Tokura, *Nature*, 2003, **426**, 55.
- 27 W. Eerenstein, N. D. Mathur and J. F. Scott, *Nature*, 2006, **442**, 759.
- 28 T. Fujii, M. Kawasaki, A. Sawa, H. Akoh, Y. Kawazoe and Y. Tokura, *Appl. Phys. Lett.*, 2005, **86**, 012107.
- 29 A. Bera, H. Peng, J. Lourembam, Y. Shen, X. W. Sun and T. Wu, *Adv. Funct. Mater.*, 2013, **23**, 4977.
- 30 R. Waser and M. Aono, *Nat. Mater.*, 2007, **6**, 833.
- 31 R. Waser, R. Dittmann, G. Staikov and K. Szot, *Adv. Mater.*, 2009, **21**, 2632.
- 32 J. W. Park, K. Jung, M. K. Yang, J.-K. Lee, D. Y. Kim and J. W. Park, *J. Appl. Phys.*, 2006, **99**, 124102.
- 33 Y. Shao, Z. Xiao, C. Bi, Y. Yuan and J. Huang, *Nat. Commun.*, 2014, **5**, 5784.
- 34 S. D. Stranks, G. E. Eperon, G. Grancini, C. Menelaou, M. J. P. Alcocer and T. Leijtens, *Science*, 2013, **342**, 341.
- 35 G. Konstantatos, M. Badioli, L. Gaudreau, J. Osmond, M. Bernechea and F. P. G. de Arquer, *Nat. Nanotechnol.*, 2012, **7**, 363.
- 36 Y. Lin and X. Guo, *Small*, 2015, **11**, 2856.